J Solid State Electrochem (2012) 16:3603–3610
DOI 10.1007/s10008-012-1792-6

ORIGINAL PAPER

Investigation of an impedancemetric NO_x sensor with gold wire working electrodes

Jonathan M. Rheaume · Albert P. Pisano

Received: 2 April 2012 / Revised: 18 May 2012 / Accepted: 29 May 2012 / Published online: 23 June 2012

Abstract Sensors that detect NO_x by a change in impedance were fabricated with gold wire electrodes and YSZ electrolyte. The effects of temperature, NO_x species, flow rate, and cross sensitivity to O_2 were quantified and evaluated. The largest phase angle shift due to NO_x was found at the lowest temperature investigated (600 °C). Linear relationships existed between the shift in phase angle and NO_x quantity up to 100 ppm. NO_2 evoked a larger response than NO at 650 °C. A reversible poisoning effect was observed following exposure to NO_2. The sensing impedance signal at 10 Hz was invariant to total flow rate. Cross sensitivity to O_2 was noted. Although O_2 evoked a much smaller response than NO_x, the larger quantity of O_2 of lean exhaust necessitated compensation.

Keywords Impedancemetric NO_x sensor · Electrochemical impedance spectroscopy (EIS) · Yttria-stabilized zirconia (YSZ)

Abbreviations

EIS	Electrochemical impedance spectroscopy
NO_x	Nitrogen oxides
YSZ	Yttria-stabilized zirconia

J. M. Rheaume (✉)
United Technologies Research Center,
East Hartford, CT, USA
e-mail: jrheaume@alum.mit.edu

A. P. Pisano
University of California, Berkeley,
Berkeley, CA, USA

Introduction

Diesel engines operate more efficiently than gasoline engines on account of the larger compression ratio, however, diesels tend to emit more particulates and nitrogen oxides (NO_x) [1]. The particulates result from poor mixing and incomplete, non-stoichiometric combustion and the attendant slower flame velocities. The lower flame temperatures of diesels due to dilution in excess air result in less NO_x than with gasoline engines, however, the three-way catalytic converter is ineffective at reducing NO_x in the presence of excess air [2, 3]. Selective catalytic reduction [4] and NO_x adsorption are means to clean up NO_x emissions [5].

The US Environmental Protection Agency has proposed regulations requiring that a NO_x sensor monitor the operation of the NO_x cleanup unit of heavy duty diesel vehicles [6]. Commercial NO_x sensors for diesel exhaust analysis consist of multiple electrochemical cells in series: the first amperometric cell removes O_2 so that a subsequent one can detect NO_x concentration indirectly. This occurs by dissociating the NO_x into O and N_2 and measuring the pumping current resulting from oxygen [7]. Automobile manufacturers have expressed the concern that commercially available NO_x sensors do not detect accurately enough at the single parts per million (ppm) level to comply with proposed regulations [8].

Impedancemetric gas sensors for NO_x detection [9–24] have shown promise for accurate NO_x detection at the single ppm level [12, 14, 19]. They operate on the principle that certain gases influence the impedance of an electrochemical cell at low frequencies ($f \leq 100$ Hz). Select gases participate in electrochemical reactions in which electron transfer alters the conductivity of the sensor. An impedance measurement

detects this electron transfer and can be correlated to the concentration of gaseous analyte species. A recent review paper summarizes work on impedance-type sensors [25].

Impedance-based detection takes place by applying an alternating voltage at a specific frequency and then recording the resulting current signal. Impedance is calculated as the ratio of small signal voltage over current. By sweeping a range of frequencies and plotting the impedances on a Nyquist plot, the arcs that result reveal information about the electrochemical system and about species concentration. The phase angle characterizes the lag or the lead between the voltage and current signals. Exposure to reactive gases evokes changes in the magnitude (modulus) and phase angle of the impedance at low frequencies ($f \leq 1$ kHz). Studies have shown the modulus to be less sensitive than the phase angle [14, 26].

The noble metals Pt and Ag are generally unsuitable electrode materials for NO_x detection because NO_x does not evoke changes in their impedance spectra at low frequencies [18, 27]. No low-frequency processes associated with a time-constant relaxation occur, making them insensitive to NO_x. Gold electrodes, however, demonstrate predictable changes in low-frequency behavior that can be correlated to the concentration of NO_x species [16–19]. This electrochemical system has also shown sensitivity to oxygen [28, 29].

The NO_x sensors under investigation in this work consist of solid gold wire working electrodes in contact with a porous, fully stabilized electrolyte layer. The counter electrode consists of porous Pt. These elements are stacked vertically on a tile of pre-fired, dense alumina (Fig. 1). Leads of porous Pt provide a conduction path to the edge of the tile, where they connect with wires to interrogate the cell (not shown).

This investigation has the specific objectives of exploring the performance of impedance-based sensors with gold electrodes. In specific, the following treatise examines how the phase angle is affected by temperature, NO_x concentration (<100 ppm), and flow rate. It also includes an examination of the relative effects of O_2, NO, and NO_2 concentrations on phase angle.

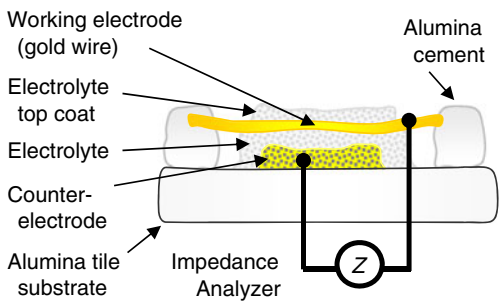

Fig. 1 Schematic cross section of a NO_x sensor with Au wire electrodes (not to scale)

Experimental

Sensors were constructed on 1 cm^2 dense alumina substrates by painting leads of platinum ink (Engelhard 6082) in parallel stripes 1 mm wide and 1 mm apart. The substrates were fired at 1,200 °C for 2 h in air inside a Thermolyne muffle furnace. A low thermal ramp rate was followed early in the firing cycle to accommodate the burnout of organic species. Subsequently, an electrolyte layer of zirconia fully stabilized by yttria (8 mol% Y_2O_3) was applied as a slurry on top of one platinum stripe (counter electrode). Upon drying, the working electrode was formed by placing gold sensing wires measuring 10 mm in length and 0.25 mm in diameter on top of the electrolyte. Alumina cement (Aremco Resbond 920) anchored them to the alumina tile. The sensing wires were attached to the other platinum lead using gold/palladium conductive paste (Engelhard A3770). The sensing wires were further coated with three coats of electrolytic slurry. This layer is porous after firing. It serves to increase the electrode-electrolyte interface and thereby enhances detection of analyte species. The sensors were dried in air, and then fired at 1,000 °C for 2 h. Care was taken to ramp the temperature gradually for organic species burn out. The sensor electrodes were attached to lead wires of gold.

The sensors were then loaded into a quartz tube for analysis by electrochemical impedance spectroscopy (EIS). Several investigations were performed, including a study of temperature dependence (600–700 °C), the effects of NO and NO_2 individually (0, 25, 50, and 100 ppm), the influence of variable flow rate (100–500 standard cubic centimeters per minute (sccm)), and the response due to O_2 (4–19 %). Unless otherwise noted, all experiments were performed at 650 °C in 500 sccm of 10 % O_2 with balance N_2. This gas composition was selected to highlight the lean nature of diesel exhaust. Although the amount of O_2 varies widely over a diesel driving cycle, 10 % was selected as a standard in order to enable comparison of results with different amounts and types of NO_x. Frequency sweeps between 1 MHz and 1 Hz were performed at 25 mV excitation amplitude. The impedance response was recorded using a Solartron Analytical SI 1260 impedance/gain-phase analyzer in combination with a Solartron Analytical SI 1287 electrochemical interface. ZPlot data acquisition software (Scribner Associates, Inc.) controlled the data collection process. A two electrode configuration was employed. Ten measurements per decade were recorded. At least 3 min elapsed after changing experimental conditions in order to ensure steady state. Two sweeps were performed for each sensor at each flow rate, gas composition, and temperature. Overlap of the two resulting impedance spectra on a Nyquist plot confirmed repeatable measurements under steady-state conditions.

A typical Nyquist plot consists of two arcs: a small high-frequency arc and a larger low-frequency arc offset from the ordinate (Fig. 2). The diameter of each semicircular arc reflects the resistance of the process(es) associated with each arc. The high-frequency arc characterizes electrolyte conductivity; it is invariant to gaseous species. On the other hand, the low-frequency arc shifts due to a mass transfer or interfacial process that is facilitated by the presence of NO_x. Nyquist plots are explained in greater detail in the literature in the context of gas sensing [25].

Phase angles were used to evaluate sensor performance. To detect species, differences in phase angle were calculated with data at 10 Hz by subtracting the phase angles obtained with and without analyte gas. This difference was related to species concentration.

EIS studies were performed on the NO_x sensor to investigate the effects of temperature, species concentration, flow rate, and cross sensitivity to O_2. Temperature was examined from 600 to 700 °C with 100 ppm NO. The sensing responses to NO and NO_2 from 0 to 100 ppm in 10 % O_2 and balance N_2 were investigated. Sensitivity to flow rate was characterized with a gas mixture consisting of 10 % O_2 with 100 ppm NO and balance N_2 from 100 to 500 sccm. Bottles of 1,000 ppm NO_x in N_2 were diluted with air and N_2 to obtain the desired amount. In investigating cross sensitivity to O_2, sensor responses due to various concentrations of O_2 from 4 to 18.9 % in balance N_2 were recorded.

Results and discussion

Data obtained by recording the impedance response of each sensor to various influences was analyzed by making Nyquist plots and by calculating phase angles.

Effect of temperature

Temperature affects both arcs. The high-frequency arc that represents electrolyte resistance shrinks with increasing temperature. Since these arcs are linked, the phase angle at the low sensing frequency of 10 Hz is also affected. Therefore the temperature must be fixed or known in order to consistently analyze the low-frequency arc. Gas-sensing relies on calibration to known gas concentrations at specific temperatures.

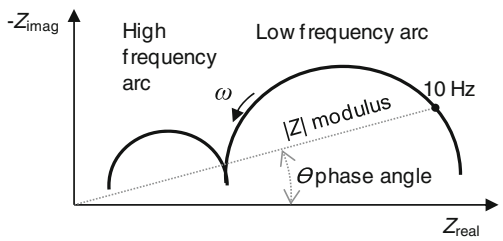

Fig. 2 Typical Nyquist plot

Sensitivity to 100 ppm NO decreased with increasing temperature as measured both by change in modulus and by phase angle shift at 10 Hz (Fig. 3). This finding may be due to the slow kinetics of oxygen reactions (reduction and incorporation in to lattice) at $T \leq 600$ °C. As a result, the effects of the free radicals NO and NO_2 that readily reduce to oxygen are more readily detected [12].

Unfortunately, the signal becomes noisy at lower temperatures. Sometimes the arc departs from a smooth, continuous curve as the effects of heterogeneities become more pronounced. The selection of a 650 °C temperature for most measurements represents a balance of sensitivity and noise.

Phase angle is linearly related to temperature at 10^5 Hz. (Fig. 4). As expected, NO_x did not affect the phase angle at this frequency. This proportional relationship may allow a NO_x sensor to be calibrated for simultaneous use as a temperature sensor as long as it is microstructurally stable. Protracted heat treatment has been reported to engender microstructural changes in the sensor [30] that alter the impedance spectrum. Aging effects were observed in the sensors over the course of days. Murray et al. noticed significant change in impedance after 11 days of testing [15]. The drift in the phase response was attributed to material instability. Temperature dependence and signal drift must be addressed for a viable NO_x sensor.

NO_x detection

Sensors were exposed to NO and NO_2 at 0, 25, 50, and 100 ppm. An in-depth study of NO was made because NO is found in much larger quantities than NO_2 in diesel exhaust [1]. Additional concentrations of NO (30, 40, and 75 ppm) were investigated. This allowed an examination in detail of the relationship between phase angle difference and NO concentration. The Nyquist plots for NO and NO_2 are shown

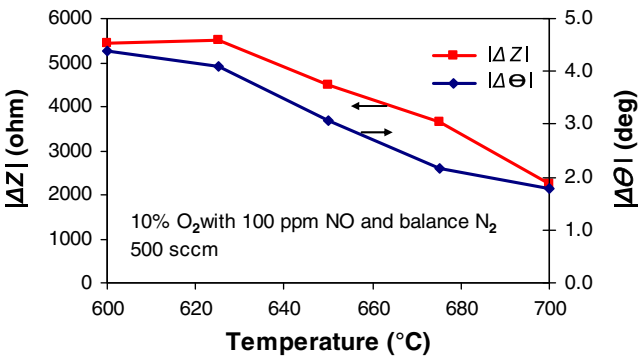

Fig. 3 Changes in modulus and phase angle at 10 Hz due to 100 ppm NO

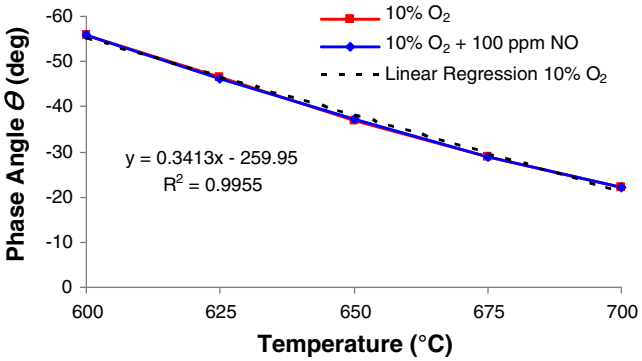

Fig. 4 Phase angles at 10^5 Hz vs. temperature

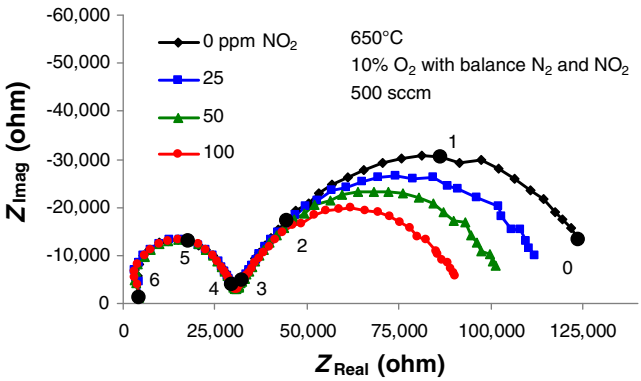

Fig. 6 Change in sensor impedance response with NO_2 content

in Figs. 5 and 6, respectively. Arabic numerals indicate the log of the interrogation frequency. For reference, each decade of frequency is indicated for the base case (10 % O_2/N_2) by filled circles.

The Nyquist plots exhibit two arcs. The semicircular form of the high-frequency arcs (f>10 kHz) indicates a single activation-energy controlled relaxation process [26] such as electrolyte conductivity [23, 31]. The kinetics of electrolytic conduction occur on a microsecond to millisecond timescale, which corresponds to the megahertz to kilohertz frequencies of the high-frequency arc. The arcs are depressed, which suggests an inhomogeneity in a physical property such as conductivity. A kink in the semicircle can be seen in the highest frequency measurements. Often a startup transient occurs during the first measurements of a series [26]. This aberration has been ascribed to the leads [32, 33]. Consistent with electrolyte conductivity, the high-frequency arcs are invariant to gaseous species. The low-frequency arcs (f<1 kHz) are affected by NO_x, in accordance with previous findings [9–11, 15, 17–19, 22]. In specific, NO_x alters the impedance response of the sensor at low frequencies. The low-frequency arcs shift inward for both NO and NO_2. The decrease in impedance stems from a rate-limiting transport process (e.g., adsorption, diffusion, and charge transport) [9, 10, 23, 34, 35]. These processes take place over a timescale of milliseconds to seconds, which corresponds to the kilohertz to single hertz frequencies of this arc.

NO_2 evokes a larger shift than an equivalent concentration of NO when evaluated at 650 °C. The larger signal from NO_2 might be attributed to the additional electron transfer associated with the reduction of NO_2. In contrast, Miura et al. reported nearly identical responses to NO and to NO_2 at 700 °C allowing total NO_x detection regardless of their relative concentrations [9, 10, 36]. This finding may result from thermodynamic equilibrium that establishes itself at increasing temperatures above 600 °C in which NO_2 over 90 % dissociates to NO and O_2 in the gas phase [12, 17]. In this study, at 650 °C the decomposition is not as complete as at 700 °C. Some NO_2 participates in electrochemical reactions on the surface of the sensor where it affects the low-frequency arc. In specific, the NO_2 reduces to NO in addition to O. Both of these species may further participate in electrochemical reactions that impact the cell impedance and thus contribute to the larger shift of the low-frequency arc due to NO_2.

From the impedance data, phase angle differences at 10 Hz were calculated. A linear relationship exists between the change in phase angle and NO_x concentration below 100 ppm, as demonstrated in Fig. 7 for both NO and NO_2.

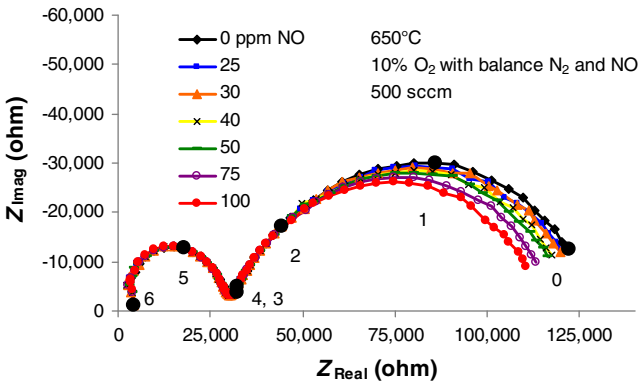

Fig. 5 Change in sensor impedance response with NO content

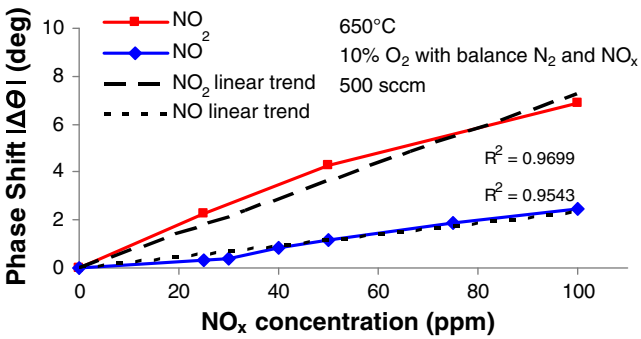

Fig. 7 Variation in phase angle difference ($\Delta\theta$) at 10 Hz with NO_x content

The former evokes smaller phase angle shifts than the latter in accordance with the shifts of the respective low-frequency arcs. Linear regressions of experimental data had high R^2 values, indicating a good fit. These trend lines had a slightly better fit when they were not restrained to pass through the origin, however, a practical sensor would require an intercept through the origin in order to function at low concentrations. Martin et al. reported linear relationships between phase angle shift and NO_x concentration from 8 to 50 ppm over a wide range of O_2 concentrations; these lines generally passed through the origin [14]. Although the empirical results presented here show promise for a sensor that can be calibrated to NO_x concentration, a more in-depth analysis with additional data points at low NO_x concentrations is necessary to be conclusive. Limitations of the experimental setup precluded an examination of NO_x concentrations less than 25 ppm.

A phenomenon was observed following the experiments with NO_2 in which the sensor required a protracted time to recover from the exposure to NO_2. The low-frequency arc of the impedance spectrum shifted inwards due to NO_2 as seen in Fig. 6, but after the NO_2 supply was shut off, the arc did not immediately return to the same position as before exposure to NO_2. Rather, the low-frequency arc shifted outwards following NO_2 exposure. During this time, the base case gases flowed (10 % O_2 in N_2, 0 ppm NO_x). This effect was transient and repeatable. Figure 8 shows the recovery of the impedance spectrum. Over 2.5 h, the low-frequency arc shifted back inwards. Eventually the entire spectrum overlapped the pre-exposure case. This temporary poisoning effect may be caused by species that reversibly adsorb on sites of electrochemical reactions and thereby impede reactions. NO did not evince this behavior. The more complex reduction mechanism of NO_2 may involve intermediary species that do not completely dissociate or desorb immediately. Woo et al. report that Au is not catalytically active enough for complete NO_2 dissociation [17], and that a catalyst is necessary for complete decomposition of NO_2 at $T \leq 700$ °C [37]. These findings support the hypothesis that NO_2 or a byproduct of its incomplete decomposition adsorbs on the sensor.

The poisoning effect was not observed with NO, however, West et al. reported a recovery period after exposure to NO using oxide electrodes [38]. The time decreased with increasing temperature. In this study, increasing the temperature to 800 °C following NO_2 exposure did not bring about an immediate recovery. This temporary poisoning effect might be circumvented by shifting NO_2 to NO at increased temperature using a rhodium catalyst before sensing, however, no investigation thereof is made here.

Flow rate

The effect of flow rate on sensor output was examined in order to determine if diffusion through the boundary layer would be affected by normal variation of exhaust flow. A mixture of 10 % O_2 with 100 ppm NO evoked the same impedance response from 100 to 500 sccm (Fig. 9). Whereas the high-frequency arcs overlap regardless of gas mixture, here the species-sensitive low-frequency arcs (f<1 kHz) overlap as well. Impedance measurements are independent of flow rate; they depend only on the composition of the mixture. Nakatou and Miura found similar results for an impedance-based sensor for a different analyte gas [39].

Cross sensitivity

In addition to NO_x species, the sensor responds to the excess O_2 that is likely to be found in diesel exhaust. It might also be sensitive to CO and hydrocarbons, but the location downstream of an oxidation catalyst may mitigate these concerns. This section explores the effect of the excess O_2 and compares the sensor output to O_2 and NO_x species.

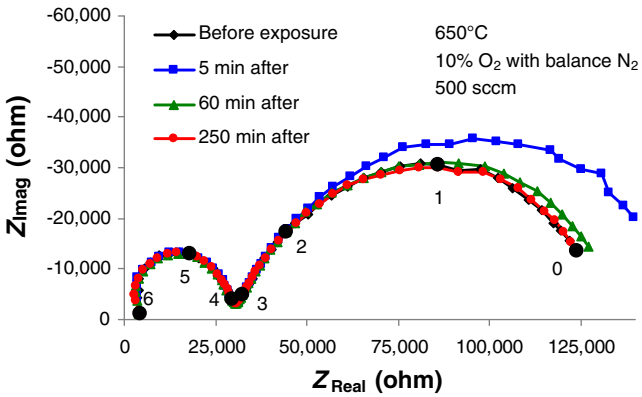

Fig. 8 Nyquist plot detailing recovery of sensor to NO_2

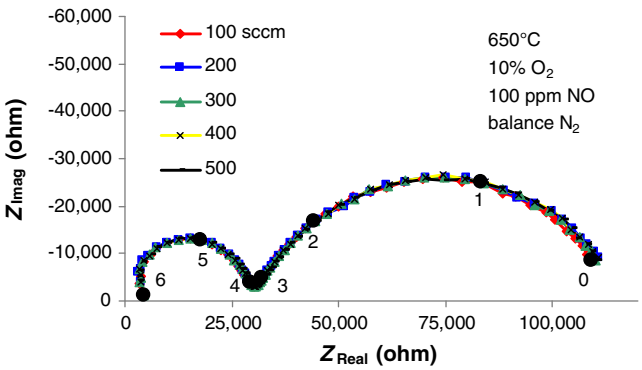

Fig. 9 Impedance response due to flow rate

Effect of O_2

Changing the O_2 concentration shifts the low-frequency arc inwards (Fig. 10) as did NO_x. Filled circles on the spectra indicate decades of frequency for the lowest O_2 concentration. The low-frequency arcs reflect a rate-limiting transport process associated with O_2 reduction. This cross sensitivity to O_2 indicates that NO_x reduction is an intermediate step of the NO_x sensing mechanism.

Mitigation of cross sensitivity to O_2 might be achieved by operating the sensor in an anoxic environment. In practice, this might be realized by replacing the second pumping cell of a conventional amperometric NO_x sensor with an impedance-based one.

The high-frequency arcs in Fig. 10 are identical regardless of gas concentration, as expected. A high-frequency arc may represent ion transport within the bulk of the electrolyte [23] or within the electrode [10].

In the literature, significant cross sensitivity to O_2 has been reported with impedancemetric sensors [13–18]. The O_2 changes the modulus, $|Z|$, which has been linearly correlated with concentration [40].

Relative effects of NO_x and O_2

The same quantity of O_2, NO, and NO_2 at 650 °C evoke different responses. Alternately, a similar response can be had with different amounts of these gases. Adding 25 ppm NO_2 or 100 ppm NO to a 10 % O_2 gas mixture has approximately the same effect as adding an additional 6 % O_2. Figure 11 shows the overlapping low-frequency arcs that demonstrate this case. The NO_x species evoke a response that is several orders of magnitude larger than an equivalent amount of O_2 because they are free radicals. The unpaired electron causes them to react with other species more readily than relatively stable O_2. For this reason, orders of magnitude more O_2 are required to equal the response of NO_x, confirming results in the literature [17]. Of NO and NO_2, the latter is less stable [3] and evokes a larger response.

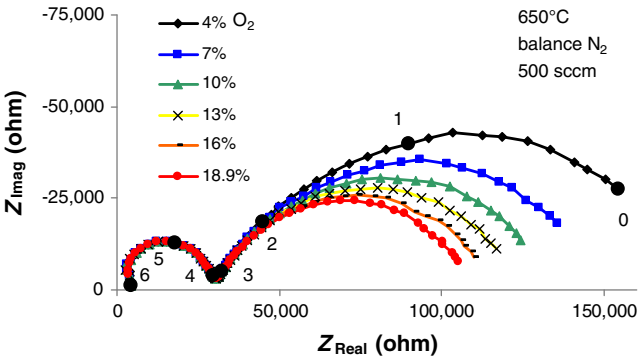

Fig. 10 Effect of O_2 concentration on Nyquist plot

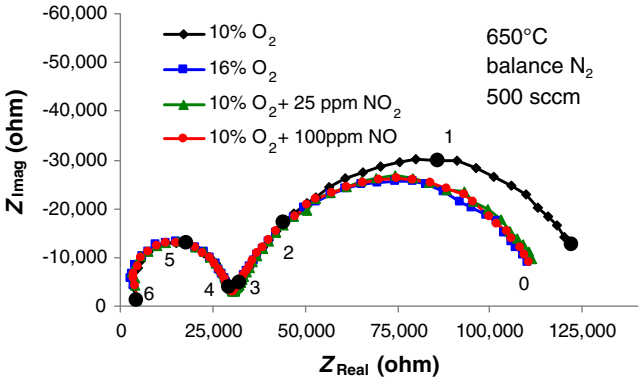

Fig. 11 Equivalent impedance response for different amounts of O_2, NO, and NO_2

Some sources report impedancemetric sensors with nearly identical responses to both NO and NO_2 enabling total NO_x sensing. They generally operate at a specific temperature [9, 10, 17, 36]. It is unclear, however, whether the equivalent sensitivity is due to the detection capability of the sensor or due to the natural thermal equilibrium shift of NO_2 to NO. At $T>600$ °C, NO_x in exhaust gases equilibrates so that the mixture consists primarily of NO (>90 %) [12]. In order to address the different responses of NO and NO_2 over a range of temperatures, a catalyst might be used to shift all NO_x to one species.

The effect of O_2 and 100 ppm NO on phase angle at 10 Hz was examined over a wide range of P_{O_2}. Figure 12 shows the phase angles obtained with 100 ppm NO and without, as well as the difference between the two. For both O_2/N_2 and 100 ppm NO in O_2/N_2, a kink can be seen at 10 % O_2. As concentration increases, the magnitude of the phase angle decreased. This trend can be more easily seen in the $\Delta\theta$ plot. The difference represents the change in phase angle at 10 Hz due to 100 ppm NO. The magnitude of the change is larger at lower P_{O_2}, however, it flattens out at larger P_{O_2}. NO and O_2 may compete for reaction sites, and a saturation effect may be seen at larger P_{O_2}. The effect is small, however, which invites further investigation.

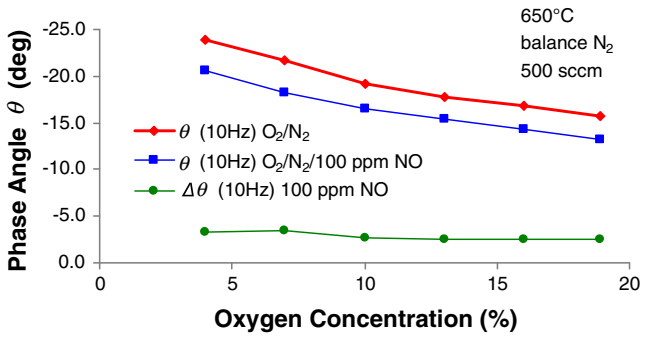

Fig. 12 Effect of 100 ppm NO on phase angle at 10 Hz vs. P_{O_2}

Summary

Sensors with gold wire working electrodes were fabricated and evaluated using impedance methods. The sensors were analyzed over a range of temperatures, NO_x concentrations, flow rates, and background O_2 concentrations.

At the low end of the investigated temperature range, the sensors were most sensitive to 100 ppm NO. The phase angle at 10^5 Hz was linearly related to temperature, independent of gas species, allowing the signal to serve as a proxy for a temperature measurement.

A linear relationship between NO_x concentration and phase angle shift at 10 Hz has been observed up to 100 ppm. NO_2 evoked a larger response than an equivalent amount of NO at 650 °C. Exposure to NO_2 required a protracted recovery period of the low-frequency arc perhaps due to a reversibly adsorbed species that blocks reaction sites.

Experimental results suggest that NO and O_2 compete for reaction sites on account of a smaller phase angle shift due to 100 ppm NO at higher O_2 concentrations. The sensors were more sensitive to NO and to NO_2 than to O_2 by several orders of magnitude, as measured by the difference in phase angle obtained at 10 Hz. An O_2 compensation scheme is necessary since O_2 is typically present in lean exhaust in quantities orders of magnitude larger than NO_x.

The performance of gold sensing electrodes is promising, however, drawback exist. Noble metals are costly. The coefficient of thermal expansion of gold differs from both the YSZ electrolyte and the alumina substrate. The melting temperature of gold prevents the cofiring of the electrodes with the electrolyte in one step. Selectivity, long-term stability and supporting electronics of impedancemetric sensors remain challenges.

Acknowledgment The authors are grateful to the Lawrence Livermore National Laboratory for providing assistance with this research endeavor.

References

1. Borman GL, Ragland KW (1998) Combustion engineering. McGraw-Hill, Boston
2. Cooper BJ (1994) Challenges in emission control catalysis for the next decade. Platinum Met Rev 38:2–10
3. Burch R, Breen JP, Meunier FC (2002) A review of the selective reduction of NO_x with hydrocarbons under lean-burn conditions with non-zeolitic oxide and platinum group metal catalysts. Appl Catal B Environ 39:283–303
4. Johnson T (2009) Review of diesel emissions and control. Int J Engine Res 10(5):275–285. doi:10.1243/14680874JER04009
5. Rajaram RR, Poulston S (2007) NO_x-trap. US Patent 7287370
6. US Environmental Protection Agency (2008) Regulations Requiring Onboard Diagnostic Systems on 2010 and Later Heavy-Duty Engines Used in Highway Vehicles Over 14,000 Pounds; Revisions to Onboard Diagnostic Requirements for Diesel Highway Vehicles Under 14,000 Pounds Summary and Analysis of Comments. EPA-420-R-08-018. Available at: http://www.epa.gov/obd/regtech/420r08018.pdf. Accessed 10 Nov 2009
7. Marek J, Trah HP, Suzuki Y, Yokomori I (eds) (2003) Sensors for automotive applications, vol 4. Wiley, New York
8. California Air Resources Board (2009) Staff report: initial statement of reasons for proposed rulemaking—technical status and revisions to malfunction and diagnostic system requirements for heavy-duty engines (HD OBD) and passenger cars, light-duty trucks, and medium-duty vehicles and engines (OBD II). Available at: http://www.arb.ca.gov/regact/2009/hdobd09/obdisor.pdf. Accessed 28 Oct 2009
9. Miura N, Nakatou M, Zhuiykov S (2002) Impedance-based total-NO_x sensor using stabilized zirconia and $ZnCr_2O_4$ sensing electrode operating at high temperature. Electrochem Comm 4:284–287
10. Miura N, Nakatou M, Zhuiykov S (2003) Impedancemetric gas sensor based on zirconia solid electrolyte and oxide sensing electrode for detecting total NO_x at high temperature. Sensor Actuator B Chem 93:221–228
11. Miura N, Koga T, Nakatou M, Elumalai P, Hasei M (2006) Electrochemical NO_x sensors based on stabilized zirconia: comparison of sensing performances of mixed-potential-type and impedancemetric NO_x sensors. J Electroceram 17:979–986
12. Zhuiykov S (2008) Electrochemistry of zirconia gas sensors. CRC Press, New York
13. Martin LP, Woo LY, Glass RS (2007) Impedancemetric technique for NO_x sensing using a YSZ-based electrochemical cell. Mater Res Soc Symp Proc 972:AA12–04
14. Martin LP, Woo LY, Glass RS (2007) Impedancemetric NO_x sensing using YSZ electrolyte and YSZ/Cr_2O_3 composite electrodes. J Electrochem Soc 154(3):J97–J104
15. Murray EP, Novak RF, Kubinski DJ, Soltis RE, Visser JH, Woo LY, Martin LP, Glass RS (2008) Investigating the stability and accuracy of the phase response for NO_x Sensing 5 %Mg-modified $LaCrO_3$ electrodes. ECS Trans 6(20):43–62
16. Woo LY, Martin LP, Glass RS, Gorte RJ (2007) Impedance analysis of electrochemical NO_x sensor using a Au/Yttria-stabilized zirconia (YSZ)/Au cell. Mater Res Soc Symp Proc 972:AA12–02
17. Woo LY, Martin LP, Glass RS, Gorte RJ (2007) Impedance characterization of a model Au/Yttria-stabilized zirconia/Au electrochemical cell in varying oxygen and NO_x concentrations. J Electrochem Soc 154(4):J129–J135
18. Woo LY, Martin LP, Glass RS, Wang W, Jung S, Gorte RJ, Murray EP, Novak RF, Visser JH (2008) Effect of electrode composition and microstructure on impedancemetric nitric oxide sensors based on YSZ electrolyte. J Electrochem Soc 155 (1):J32–J40
19. Woo LY, Glass RS, Novak RF, Visser JH (2010) Effect of electrode material and design on sensitivity and selectivity for high temperature impedancemetric NO_x sensors. J Electrochemical Soc 157(3):J81–J87
20. Stranzenbach M, Gramckow E, Saruhan B (2007) Planar, impedance-metric NO_x-sensor with spinel-type SE for high temperature applications. Sens Actuator B Chem 127:224–230
21. Stranzenbach M, Saruhan B (2007) Planar, impedance-metric NO_x-sensor with NiO SE for high temperature applications. In: Solid-state sensors, actuators and microsystems conference, Lyon, 10–14 June 2007. Transducers & Eurosensors '07, pp 983–986
22. Stranzenbach M, Saruhan B (2009) Equivalent circuit analysis on NO_x impedance-metric gas sensors. Sens Actuator B Chem 137:154–163
23. Wu N, Chen Z, Xu J, Chyu M, Maob SX (2005) Impedance-metric Pt/YSZ/Au–Ga_2O_3 sensor. Sens Actuator B Chem 110:49–53

24. Shimizu Y, Takase S, Koba D (2008) A NO_x sensor based on solid-electrolyte impedance transducer. Adv Mater Res 47–50:479–482
25. Rheaume JM, Pisano AP (2010) A Review of recent progress in sensing of gas concentration by impedance change. IONICS-2010-0148
26. Orazem M, Tribollet B (2008) Electrochemical impedance spectroscopy. Wiley, New Jersey
27. Barsoukov E, Macdonald JR (eds) (2005) Impedance spectroscopy: theory, experiment, and applications, 2nd edn. Wiley, New Jersey
28. van Hassel BA, Boukamp BA, Burggraaf AJ (1991) Electrode polarization at the Au, $O_{2(g)}$/yttria stabilized zirconia interface. Part I: theoretical considerations of reaction model. Sol Stat Ion 48:139–154
29. van Hassel BA, Boukamp BA, Burggraaf AJ (1991) Electrode polarization at the Au, $O_{2(g)}$/yttria stabilized zirconia interface. Part II: electrochemical measurements and analysis. Sol Stat Ion 48:155–171
30. Kondoh J, Kawashima T, Kikuchi S, Tomii Y, Ito Y (1998) Effect of aging on yttria-stabilized zirconia I. A study of its electrochemical properties. J Electrochem Soc 145(5):1527–1536
31. Yoon JW, Grilli ML, Di Bartolomeo E et al (2001) The NO_2 response of solid electrolyte sensors made using nano-sized $LaFeO_3$ electrodes. Sensor Actuator B Chem 76:483–488
32. Primdahl S, Mogensen M (1997) Oxidation of hydrogen on Ni/yttria-stabilized zirconia cermet anodes. J Electrochem Soc 144 (10):3409–3419
33. Hertz JL, Tuller HL (2004) Electrochemical characterization of thin films for a micro-solid oxide fuel cell. J Electroceram 13:663–668
34. Nakatou N, Miura N (2004) Impedancemetric sensor based on YSZ and In_2O_3 for detection of low concentrations of water vapor at high temperature. Electrochem Comm 6:995–998
35. Nakatou N, Miura N (2005) Detection of combustible hydrogen-containing gases by using impedancemetric zirconia-based water-vapor sensor. Sol Stat Ion 176:2411–2415
36. Miura N, Elumalai P, Plashnitsa V, Ueda T, Wama R, Utiyama M (2009) Solid-state electrochemical gas sensing. In: Comini E, Faglia G, Sberveglieri G (eds) Solid state gas sensing. Springer, New York, pp 181–207
37. Yoo J, Van Assche FM, Wachsman ED (2006) Temperature-programmed reaction and desorption of the sensor elements of a WO_3/YSZ/Pt potentiometric sensor. J Electrochem Soc 153: H115–H121
38. West DL, Montgomery FC, Armstrong TR (2005) NO-selective NO_x sensing elements for combustion exhausts. Sens Actuator B Chem 111–112:84–90
39. Nakatou N, Miura N (2006) Detection of propene by using new-type impedancemetric zirconia-based sensor attached with oxide sensing-electrode. SensActuator B Chem 120:57–62
40. Zhuiykov S, Miura N (2005) Solid-state electrochemical gas sensors for emission control. In: Sorrell CC, Nowotny J, Sugihara S (eds) Materials for energy conversion devices. Woodhead Publishing, Cambridge, pp 303–335